A LETTERS JOURNAL EXPLORING THE FRONTIERS OF PHYSICS

OFFPRINT

Dephasing due to semi-conductor charging masks decoherence in electron-wall systems

Z. CHEN and H. BATELAAN

EPL, **129** (2020) 40004

A Letters Journal Exploring the Frontiers of Physics

AN INVITATION TO SUBMIT YOUR WORK

epljournal.org

The Editorial Board invites you to submit your Letters to EPL

Choose EPL, and you'll be published alongside original, innovative Letters in all areas of physics. The broad scope of the journal means your work will be read by researchers in a variety of fields; from condensed matter, to statistical physics, plasma and fusion sciences, astrophysics, and more.

Not only that, but your work will be accessible immediately in over 3,300 institutions worldwide. And thanks to EPL's green open access policy you can make it available to everyone on your institutional repository after just 12 months.

Run by active scientists, for scientists

Your work will be read by a member of our active and international Editorial Board, led by Bart Van Tiggelen. Plus, any profits made by EPL go back into the societies that own it, meaning your work will support outreach, education, and innovation in physics worldwide.

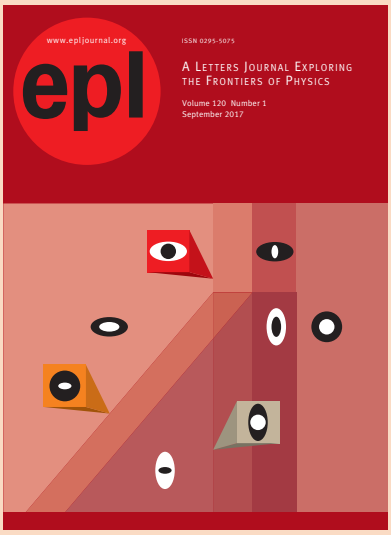

OVER

638,000

full-text downloads in 2017

Average submission to online publication

100 DAYS

21,500

citations in 2016

We greatly appreciate the efficient, professional and rapid processing of our paper by your team.

Cong Lin
Shanghai University

Four good reasons to publish with EPL

1. **International reach** – more than 3,300 institutions have access to EPL globally, enabling your work to be read by your peers in more than 90 countries.

2. **Exceptional peer review** – your paper will be handled by one of the 60+ co-editors, who are experts in their fields. They oversee the entire peer-review process, from selection of the referees to making all final acceptance decisions.

3. **Fast publication** – you will receive a quick and efficient service; the median time from submission to acceptance is 75 days, with an additional 20 days from acceptance to online publication.

4. **Green and gold open access** – your Letter in EPL will be published on a green open access basis. If you are required to publish using gold open access, we also offer this service for a one-off author payment. The Article Processing Charge (APC) is currently €1,400.

Details on preparing, submitting and tracking the progress of your manuscript from submission to acceptance are available on the EPL submission website, **epletters.net**.

If you would like further information about our author service or EPL in general, please visit **epljournal.org** or e-mail us at **info@epljournal.org**.

EPL is published in partnership with:

European Physical Society

Società Italiana di Fisica

EDP Sciences

IOP Publishing

A Letters Journal Exploring the Frontiers of Physics

February 2020

EPL, **129** (2020) 40004
doi: 10.1209/0295-5075/129/40004

www.epljournal.org

Dephasing due to semi-conductor charging masks decoherence in electron-wall systems

Z. Chen and H. Batelaan

University of Nebraska, Lincoln - Lincoln, NE 68588-0299, USA

received 30 January 2020; accepted in final form 28 February 2020
published online 23 March 2020

PACS 03.65.Ta – Foundations of quantum mechanics; measurement theory
PACS 03.75.-b – Matter waves
PACS 03.65.Vf – Phases: geometric; dynamic or topological

Abstract – In the interaction between a quantum mechanical electron wave and a wall, loss of interference contrast is observed. It is of general interest to identify the mechanism and categorize its nature as dephasing or decoherence. Decoherence is of fundamental importance for the transition between the classical and quantum boundary, while dephasing is often an experimental detriment that needs to be understood and overcome. We find that the loss of contrast is attributed to a local charge distribution induced by secondary emission: a dephasing mechanism. This mechanism is expected to be present for many materials, is clearly visible for copper oxide, and can mask decoherence mechanisms. The local charge distribution on the wall causes a loss of contrast and electron beam deformation. A model based on Coulomb interaction with the surface charge gives good agreement for both features. Our model can thus be used to improve the experimental design and lead to separate out decoherence phenomena in the electron-wall system.

Introduction. – In matter-wave interferometry, loss of contrast falls into two broad classes: that due to dephasing or decoherence. Dephasing is time-reversible while decoherence is time-irreversible [1]. Even though decoherence is ubiquitous, it is hard to create a simple and isolated environment where it can be observed [2–8]. Understanding conditions of decoherence may help to reach diffraction-limited electron microscopy [9–11] and to find solutions to its deleterious effect on quantum computing [12–14]. Coherence of electrons close to a surface in electron-on-a-chip systems [15,16] or in a quantum electron microscope [17,18] can also be affected by electron-wall decoherence. Our goal is to find an experimental system for electrons that provides a decohering environment for tests related to the quantum measurement problem [8,19]. Decoherence has been studied theoretically [9,10,20–25] and experimentally [26–30] for the electron-wall system. Hasselbach [26] reported the observation of decoherence. Decoherence can happen when imprinting which-way information onto electrons by interacting with an introduced environment [31]. In [26] the environment was a silicon surface in close proximity to the electrons. We extended this work by using silicon and metal surfaces, and modified this system by using electron diffraction instead of interferometry [27]. Our experiments on a conductive surface (gold) failed to show loss of contrast, while a semiconductive surface (silicon) produced a loss of contrast when electrons are close to the surface [27]. We compared the experimental results to a variety of theoretical models of decoherence and established that the decoherence rate was about 100 times smaller than predicted by some of the theoretical models, shedding doubt on the earlier claim [26]. The question remains, what is the physical nature of the process that causes the loss of contrast. If this mechanism can be identified and is due to dephasing, its effect may be corrected for and assist in the hunt for the decoherence mechanism. In this paper, we provide evidence that one mechanism that explains the loss of contrast is the interaction of the free electron with a charge distribution on the surface. When hit by electrons, surfaces can become positively charged by secondary emission. In this way, electrons can experience deflecting forces. The charge distribution on the surface mimics the spatial shape of the electron beam pattern and the forces act in both the vertical and horizontal directions. A semiclassical model is used to simulate diffraction and the effect of the forces. The electron diffraction is treated quantum mechanically by Fourier transformation of the position

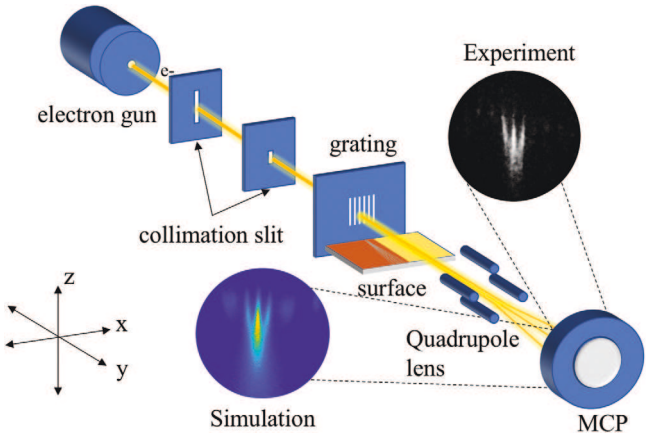

Fig. 1: Schematic experimental setup. Electrons are produced by an electron gun and are collimated by two collimation slits. The beam propagates along the longitudinal direction (y) to the diffraction grating and gets diffracted. Subsequently, the diffracted beam passes over the sample surface, half is gold coated, and half is copper oxidized. By moving the surface, the diffracted beam can interact with gold or copper oxide. An electric quadrupole lens is used to magnify the diffraction pattern in both directions. A multi-channel plate receives the electrons and produces fluorescent light which is captured by a camera. An experimental image is presented (top right) which shows a distorted diffraction pattern. The simulation result is presented at the bottom center.

distribution, while the propagation after passage through the grating is treated classically. We present the results of our model and the experimental data. Our model reproduces the features of the experimental data including the loss of contrast and distortions of the diffraction pattern. We conclude that a charge distribution that is similar to our electron beam profile causes the loss of contrast and that the charge distribution is caused by secondary emission.

Experimental setup. – Our experiment is similar to that reported in [27], except that a copper oxide surface is used to maximize possible charging effects. The relevant schematic summary of the experimental setup is now given. A coherent electron beam with energy $E = 1670\,\mathrm{eV}$ from a tip source is collimated by two collimation slits that are 25 cm far apart (fig. 1). The first slit is $12.7\,\mu$m wide and the second slit is $2\,\mu$m wide. The collimated beam propagates 6.5 cm to a diffraction grating and has a transverse coherence length of about 400 nm (and is $3.3\,\mu$m wide at the grating). The diffraction grating has open slits with widths $a = 50\,\mathrm{nm}$ and periodicity $b = 100\,\mathrm{nm}$. Thus, the electron beam coherently illuminates about 4 slits and is subsequently diffracted by the grating. After passing through the grating, electrons continue to propagate over a surface. The surface has multi-layers: the bottom layer is a square ($l = 1\,\mathrm{cm}$ side) of magnesium oxide; the middle layer is a gold coating; on the top of gold, half of the surface is sputtered with copper in an oxygen atmosphere

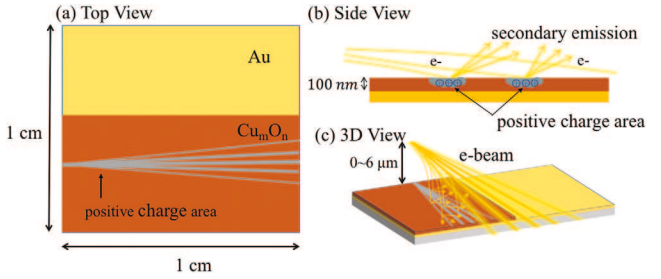

Fig. 2: Surface and secondary emission. Three different views of our sample surfaces are presented. Top view (a): the orange area is copper oxide, and the yellow area is gold for comparison. Side view (b) and 3D view (c): yellow curves represent electron trajectories and secondary emissions. Electrons hit copper oxide and cause secondary emissions which leads to a positive charge distribution on the surface. Grey lines indicate positive charge areas and mimic the diffracted electron beam pattern.

to make copper oxide. Electrons interact with the surface and pass through a quadrupole lens and a deflector. The electrons are imaged with a micro-channel plate (MCP) and camera. The whole system is contained in a vacuum of 3×10^{-7} torr and is shielded by two layers of high permeability metal to minimize the effect from the local magnetic field.

In this setup, by moving the surface vertically and horizontally, the distance between beam and surface, and the location where the beam passes over the surface can be controlled. The surface can be pulled out to characterize the undistorted beam. The angle of the surface is adjusted to make the surface nominally parallel to the electron beam and thus increase the interaction strength. The CCD camera monitors the MCP during the experiment to observe electron beam distortion and loss of contrast. A counter monitors the electron detection rate. Images and corresponding digital data from the camera are captured and processed with a LabView program.

During the experiment, electrons propagate at a velocity of $v = 2.4 \times 10^7\,\mathrm{m/s}$ over a total length of 105 cm from the source to the detector. At our count rate of 3 kHz, there is only one electron in the system at any time which avoids interaction between electrons. Given that the height of the electrons above the surface ranges from 0 to 10 microns, Coulomb interaction with the image charge is expected [32]. Also, theoretical models predict that decoherence due to image charge entanglement may play a role. Apart from electrons inducing image charges on the surface, electrons can also hit the surface and cause charging (fig. 2). Leakage current from the surface can remove this charge. Thus charging is not expected for a good conductor, and data for copper oxide can be compared to data for gold for which no distortion is observed. For a continuous electron beam close to a copper oxide surface, a steady-state charge distribution is reached. The field of this steady-state charge distribution can dephase the passing electrons via the Coulomb force, which is the main mechanism discussed in this work. On the other hand, the

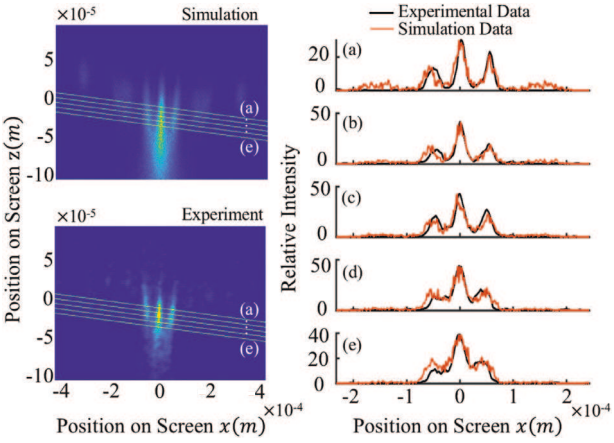

Fig. 3: Distorted diffraction pattern. The left top image is a simulated distorted diffraction pattern with the surface present, and the left bottom image is experimental data. Both diffraction patterns match each other in general shape. On the right side, line profiles (yellow cross-lines) are presented. The experimental results and simulation agree well.

image charge can decohere the electrons if entanglement is induced between the passing electrons and parts of the wall. The idea of the experiment is to compare the experimental diffraction image with a simulation that includes a reasonable electric field above the surface. Knowledge of the field can be used to correct the diffraction image and help to search for small decoherence effects that remain.

In fig. 3, the height of the surface is adjusted vertically (z-axis) in the electron beam so that the electron count is reduced to half. The surface is positioned horizontally so that a "clean" spot on the surface is found. At some locations a dust particle causes significant distortions, which are easily avoided by this horizontal adjustment. Right after the surface has been placed in the electron beam, the electrons hit the copper oxide surface, and the diffraction pattern starts to deform. After about ten minutes, the diffraction pattern becomes steady. We interpret this as a charging process that has reached its steady state and the diffraction pattern is recorded at this time. It is not possible to measure immediately upon placing the surface in the electron beam, as the diffraction pattern takes time to reach sufficient spatial resolution to measure the loss of contrast.

Since the diffraction pattern changes gradually for about ten minutes, and the flight time is $\sim 10^{-9}$ s, the image charge is not dominating this process. We hypothesize that when the surface is close to the beam, electrons are attracted due to image charge and part of the electrons crash into the surface causing secondary emissions, as shown in fig. 2, which leaves charged areas. During the surface charging, the electron beam is gradually attracted more to the surface from which we conclude that the areas become more strongly positively charged. These areas mimic the electron diffraction pattern above the surface, like a footprint, and can bend electron trajectories both in the vertical and horizontal direction.

The charged surface changes the diffraction pattern which is shown in fig. 3; the electrons passing closer to the surface are more distorted than the electron passing further from the surface. Lines are drawn at varying heights above the surface, crossing the diffraction pattern, and the corresponding intensity profiles are presented in fig. 3(a) to 3(e). Comparing those line-profiles, it is clear that the diffraction pattern's contrast declines and the peak separation reduces with the distance above the surface. Note that the noise on the experimental data is less than that in the simulation results.

Semi-classical model. – To verify our assumption that the diffraction pattern distortion is due to charging, we simulated this process using a semi-classical model. The electrons' classical trajectories, in the electric field created by positive charges on the surface, are calculated using the equation of motion

$$m\ddot{\vec{r}} = -\frac{1}{4\pi\epsilon_0}\left(\frac{e^2}{4z^2}\hat{z} + \sum_i \frac{q(\vec{r}'_i)e}{|\vec{d}_i|^2}\hat{d}\right), \tag{1}$$

where m is the mass, e is the elementary charge, ϵ_0 is the vacuum permittivity, $\vec{r} = (x, y, z)$ is the passing electron's position vector, $\vec{r}'_i = (x_i, y_i)$ is the position vector of the charge on the surface, z is the height of the passing electron, and $\vec{d}_i = \vec{r} - \vec{r}'_i$ is the vector from the charge distribution to the passing electron. The first term on the right-hand side of eq. (1) is the image charge attraction, and the second term is the force from the charge distribution on the surface. The electron initial position is chosen randomly according to a Gaussian distribution with a width of 12.6 μm in the vertical direction and 3.2 μm in the horizontal direction. The electron momentum distribution is described as

$$p(\theta) = p_0 \frac{\sin^2(\delta_1)}{\delta_1^2}\frac{\sin^2(N\delta_2)}{\sin^2(\delta_2)}, \tag{2}$$

with

$$\begin{cases} \delta_1 = \dfrac{\pi}{\lambda} a \sin(\theta), \\ \delta_2 = \dfrac{\pi}{\lambda} b \sin(\theta), \end{cases} \tag{3}$$

where $p_0 = 2.2 \times 20^{-23}\,\mathrm{kg \cdot m/s}$ is a constant, $N = 3$ is the number of coherently illuminated slits, $\lambda = 3 \times 10^{-11}$ m is the electron wavelength, θ is the angle of the initial electron momentum with respect to the y-direction in the x-y plane. The positive charge distribution is simulated by a point matrix with assigned charge values at every location $(x, y) = (x_i, y_i)$. The matrix grid has $\Delta x = 2 \times 10^{-7}$ m and $\Delta y = 10^{-6}$ m, and the distribution is

$$\begin{aligned} q(x,y) &= q_0 N(y) h(x,y) \left[\left(y + \frac{l}{2}\right) e^{k\left(y+\frac{l}{2}\right)}\right], \\ h(x,y) &= \frac{\sin^2(\delta_a)}{\delta_a^2}\frac{\sin^2(N\delta_b)}{\sin^2(\delta_b)}, \end{aligned} \tag{4}$$

with

$$\begin{cases} \delta_a = \dfrac{\pi}{\lambda} a x \Big/ \sqrt{x^2 + \left(y + \dfrac{l}{2}\right)^2}, \\ \delta_b = \dfrac{\pi}{\lambda} b x \Big/ \sqrt{x^2 + \left(y + \dfrac{l}{2}\right)^2}, \end{cases} \tag{5}$$

where x and y are coordinates shown on fig. 1 with the origin at the center of the surface. The constant q_0 has a value of 1.1×10^{-34} C, the exponential factor k is $4 \times 10^3\,\mathrm{m}^{-1}$, and $N(y) = 1/\int_{-l/2}^{l/2} h(x,y)\mathrm{d}x$ is a normalization factor which insures that the beam contains the same amount of charge at different locations y. The charge distribution described in eq. (4) shows that the most highly charged area on the surface is located at the far end of the surface (with respect to the passing electron). The maximum charge density in the simulation is $q(0, l/2)/\Delta x \Delta y$, or about $1\,\mu\mathrm{C/m}^2$, which is below the maximum charge density of a metal surface [33]. Propagating the electron momentum distribution over the surface, eq. (2), leads to an electron position distribution that leaves a charge footprint on the surface, eq. (4). Other than the lateral charge distribution that mimics the diffraction pattern, there is an extra exponential function to adjust the charge distribution in the propagation y-direction. The experimental functional dependence in the y-direction is not known. The question we want to answer is, if any reasonable charge distribution can be found to explain the distorted diffraction pattern. The answer is affirmative, and thus we cannot claim the presence of decoherence, but only dephasing, which is the main claim in this work. The exponential shape of the charge distribution was motivated by the increased exposure of the end part of the surface to the incoming electron beam, as it takes time for the image charge (and the steady state charge distribution) to attract the beam to the surface. A part of the beam collides mostly with the end part of the surface and causes charging by secondary emission, and a part of the beam passes the surface. The electron that passed the surface freely propagate for 24 cm to the detector plane to yield a distorted diffraction pattern.

We compared experimental data and simulation for the conditions that the surface is far from and close to the beam. When the surface is far from the beam, the position distribution is tilted from the horizontal. Given that the diffraction grating is nominally aligned vertically, an horizontal diffraction pattern is expected. In the simulation, a tilt correction of 0.04 rad was applied. Additionally, the image of each diffraction order is not perfectly aligned with the vertical direction. In the simulation, the oval shape of the electron beam is tilted by 0.1 rad. In the experiment, the quadrupole lens is not perfectly aligned. To overcome this problem, a coordinate transformation (correction) is made on the experimental image. To determine the transformation, a TEM grid of 127 μm square is inserted in and illuminated with a larger beam. The distorted shadow of the grid is captured and one linear coordinate

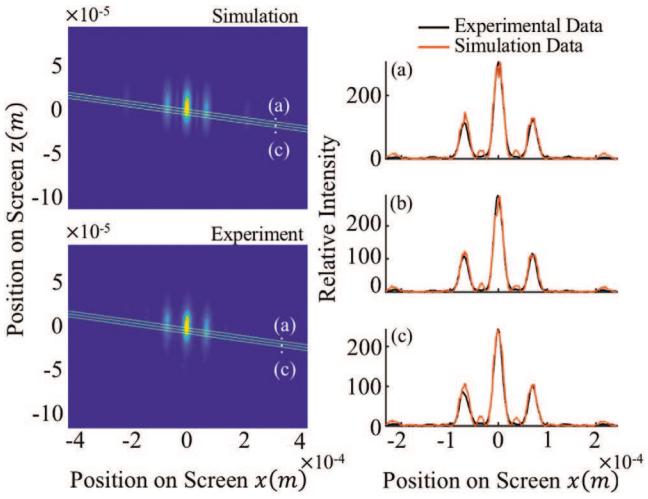

Fig. 4: Diffraction pattern without surface. In the figure, the top left and bottom left images are the simulation and experimental data. On the right side, line profiles (corresponding to the yellow lines on the left) are presented. Experimental data and simulation agree well except for small deviations between the zero and first-order peaks (see text for explanation).

transformation exists to make the grid shadow rectangular. The transformation corrects and calibrates the length scale of the image. After applying the correction to the experimental data, the diffraction patterns found are shown on the left side in fig. 3 and fig. 4. Lines are drawn perpendicularly to the center peak across the distorted diffraction pattern. The resulting line profiles are also presented in the figure. The experimental data and simulation agree well. A difference between the simulated and experimental diffraction line profiles in fig. 4 is the small peak between the zero and first-order. The simple analytical formula, used in eq. (2) to simulate the diffraction, represents equally illuminated multiple slits. However, in the experiment, the slits in the grating are not illuminated equally due to the finite electron beam width. A Gaussian-shaped envelope on slits amplitude can be used to eliminate the small peaks in the diffraction pattern.

With the surface close to the beam, the diffraction pattern shown in fig. 3 is stretched and distorted. From top to bottom, the electrons pass closer to the surface and correspondingly the distortion of the pattern increases. In the line profile on the top, the peak distance and width are mostly undisturbed. As the height of the electron above the surface is reduced, the resulting peaks converges and obscure. The line profiles are in reasonable agreement with the experimental data; right part of fig. 3. Peaks width and distance follow the same trend.

Conclusions. – In the current charge distribution model, the parameter k in eq. (4) can be adjusted. The simulated patterns are sensitive to this parameter, and only for a positive value of k, where most charges accumulate at the end of the surface, a good match with the experiment is found. Other charge distributions may also

lead to good agreement, which would lead to the same conclusion that the electron interaction can be described by dephasing, and no decoherence is needed. Given that this work is part of a search for decoherence phenomena, our current result is useful because charging due to secondary emission is likely to affect electron-wall interaction experiments with electrons in close proximity to walls made of other materials. For other materials the effect may be smaller, but should not be ignored. Dephasing due to charging can mask decoherence, if at all present, and thus needs to be identified. To learn how to do this was the objective of this study. The charging effect is expected to be strong for semi-conductors, which is why we chose a copper oxide surface. For metallic surfaces, one would expect that the steady-state charge distribution is much weaker given the high conduction. Nevertheless, continuous secondary emission remains. Metallic surface are of particular interest as decoherence theory is better established for them and an experimental study would be valuable. However, in a previous study on gold we demonstrated that the interaction between the electron and the wall is significantly weaker [27], and the identification of the mechanism was problematic. Our present study provides a pathway to identify and quantify dephasing, so that the dephasing contribution may be removed and the decoherence contribution may be measured when studying the interaction between electrons and a metallic wall.

* * *

The authors wish to thank Peter Beierle for his instructions on the experimental apparatus, Detian Yang, Bret Gergely, Sam Keramati for discussions. This work is partially done by utilizing the Holland Computing Center of the University of Nebraska, which receives support from the Nebraska Research Initiative. The research was performed in part in the Nebraska Nanoscale Facility: National Nanotechnology Coordinated Infrastructure and the Nebraska Center for Materials and Nanoscience, which are supported by the National Science Foundation under Award ECCS: 1542182, and the Nebraska Research Initiative. We gratefully acknowledge support by the U.S. National Science Foundation under Grant No. PHY-1912504.

REFERENCES

[1] Chen Z., Beierle P. and Batelaan H., *Phys. Rev. A*, **97** (2018) 043608.
[2] Schlosshauer M., *Decoherence: And the Quantum-to-Classical Transition* (Springer, Berlin) 2007.
[3] Joos E., Zeh H. D., Kiefer C., Giulini D. J., Kupsch J. and Stamatescu I. O., *Decoherence and the Appearance of a Classical World in Quantum Theory* (Springer, New York) 2013.
[4] Buchleitner A., Viviescas C. and Tiersch M., *Entanglement and Decoherence: Foundations and Modern Trends* (Springer) 2008.
[5] Weinberg S., *Lectures on Quantum Mechanics* (Cambridge University Press) 2015.
[6] Zurek W. H., *Phys. Today*, **44** (1991) 36.
[7] Zurek W. H., *Los Alamos Sci.*, **27** (2002) 86.
[8] Zurek W. H., *Phys. Today*, **67** (2014) 44.
[9] Howie A., *Ultramicroscopy*, **111** (2011) 761.
[10] de Abajo F. G., *Phys. Rev. Lett.*, **102** (2009) 237401.
[11] Uhlemann S., Müller H., Zach J. and Haider M., *Ultramicroscopy*, **151** (2015) 199.
[12] Pellizzari T., Gardiner S. A., Cirac J. I. and Zoller P., *Phys. Rev. Lett.*, **75** (1995) 3788.
[13] Byrd M. S. and Lidar D. A., *Phys. Rev. Lett.*, **89** (2002) 047901.
[14] Ladd T. D., Jelezko F., Laflamme R., Nakamura Y., Monroe C. and O'Brien J. L., *Nature*, **464** (2010) 45.
[15] Hammer J., Thomas S., Weber P. and Hommelhoff P., *Phys. Rev. Lett.*, **114** (2015) 254801.
[16] Zimmermann R., Weber P., Seidling M. and Hommelhoff P., *Appl. Phys. Lett.*, **115** (2019) 104103.
[17] Putnam W. P. and Yanik M. F., *Phys. Rev. A*, **80** (2009) 040902.
[18] Kruit P., Hobbs R. G., Kim C.-S., Yang Y., Manfrinato V. R., Hammer J., Thomas S., Weber P., Klopfer B., Kohstall C. *et al.*, *Ultramicroscopy*, **164** (2016) 31.
[19] Schlosshauer M., *Rev. Mod. Phys.*, **76** (2005) 1267.
[20] Machnikowski P., *Phys. Rev. B*, **73** (2006) 155109.
[21] Scheel S. and Buhmann S. Y., *Phys. Rev. A*, **85** (2012) 030101.
[22] Anglin J., Paz J. and Zurek W., *Phys. Rev. A*, **55** (1997) 4041.
[23] Ford L., *Phys. Rev. D*, **47** (1993) 5571.
[24] Schwinger J., *Phys. Rev.*, **158** (1967) 1391.
[25] Mazzitelli F. D., Paz J. P. and Villanueva A., *Phys. Rev. A*, **68** (2003) 062106.
[26] Sonnentag P. and Hasselbach F., *Phys. Rev. Lett.*, **98** (2007) 200402.
[27] Beierle P. J., Zhang L. and Batelaan H., *New J. Phys.*, **20** (2018) 113030.
[28] Kerker N., Röpke R., Steinert L.-M., Pooch A. and Stibor A., arXiv preprint, arXiv:2001.06154 (2020).
[29] Hsiang J.-T. and Lee D.-S., *Phys. Rev. D*, **73** (2006) 065022.
[30] Röder F. and Lubk A., *Ultramicroscopy*, **146** (2014) 103.
[31] Zurek W. H., *Rev. Mod. Phys.*, **75** (2003) 715.
[32] Barwick B., Gronniger G., Yuan L., Liou S.-H. and Batelaan H., *J. Appl. Phys.*, **100** (2006) 074322.
[33] Wang S., Xie Y., Niu S., Lin L., Liu C., Zhou Y. S. and Wang Z. L., *Adv. Mater.*, **26** (2014) 6720.